Fusion Engineering Windtunnel Experiment

INDI vs. PID

T. Koning

May, 2022

Abstract

This experiment compares the wind disturbance rejection of PID and INDI control algorithms of the Fusion Engineering Reflex flight controller. Wind disturbance rejection is tested with wind speeds of *10 m/s*, *15 m/s*, *20 m/s* and *25 m/s*. The experiment is conducted within the TU Delft windtunnel facilities. Performance is measured with two metrics: 'relative maximum position error' e_{rel} and 'relative integrated error' I_{rel}. The first metric e_{rel} shows the ratio of the maximum position error due to the wind gust for both algorithms, where the second metric I_{rel} is ratio of the integrated error of both algorithms, which takes into account the recovery time of the drone. INDI outperforms PID at every wind speed. The larger the windspeed is, the more INDI outperfroms PID. At the maximum wind speed of 25m/s, INDI was able to recover its position, while PID was fighting the gust until the battery was depleted. This shows that INDI has the potential to make drones fly in more extreme wind conditions.

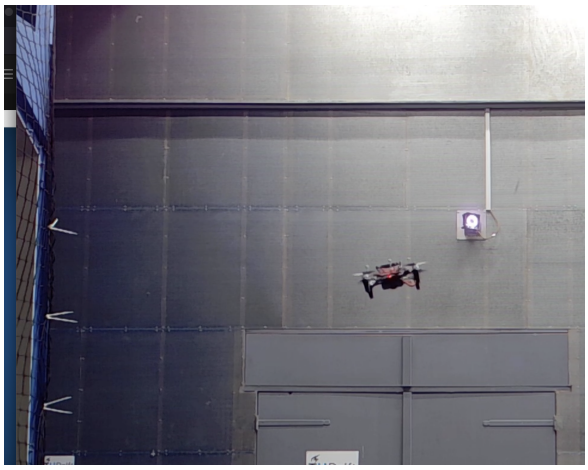

Figure 1: Drone with Fusion Reflex flight controller flying in the wind gust

1. Introduction

1.1. Fusion Engineering's Reflex

Fusion Engineering is working to create the most reliable, flexible and easy-to-use flight controller for any type of multirotor drone. Where conventional flight controllers use Proportional-Integral-Derivative control (PID control), Fusion's flight controller uses a technique based on Incremental Nonlinear Dynamic Inversion (INDI): A novel method designed at TU Delft that overcomes the robustness issues of NDI by reducing the dependency on an accurate system model while still allowing for a precise and fast response.

1.2. Experiment goal

The goal of this experiment is to compare the response to wind gust disturbance of INDI to that of PID by applying a wind gust to the drone.

2. Method and Equipment

2.1. Equipment

For this experiment, the wind tunnel facility of the Technical University of Delft is used. This wind tunnel allows for accurate wind speeds and laminar flow. The wind tunnel has an optitrack system installed. The optitrack system consists of a set of twelve cameras with a ring of light bulbs emitting infrared light. The drone is outfitted with four infrared reflecting balls, that reflect the emitted light back to the cameras. The optitrack software is capable of reconstructing position and orientation of the drone based on this information. This information is sent from the optitrack computer to the drone's flight controller using a HolyBro V3 SiK telemetry module. The Fusion Reflex flight controller uses this sensor information as an input to the flight control algorithm.

The drone frame uses the Iflight XL7 frame as basis, but uses a custom 3D printed top plate, designed to hold the reflecting balls for the optitrack system. The propellers are Dalprop T5249C. The motors are T-motor Velox V2.0 2207 2550kV. The ESC's are Aikon BLheli-32 30A ESC's.

2.2. Trajectory relative to the wind turbine

Because we want to test wind gust rejection, we want to have a fast change from low to high wind speed. We program the drone to follow a trajectory in which the drone takes off in a (close to) no-wind area outside the openening of the wind tunnel, after which it flies in a direction perpendicular to the wind speed into the wind gust. Each trajectory setpoint has a hold time of *10 seconds*.

The setpoints (X, Y, Z) in meters are

- setpoint 1: (0, 2.5, 0)
- setpoint 2: (0, 2.5, 3)
- setpoint 3: (0, 0, 3)
- setpoint 4: (0, 2.5, 3)
- setpoint 5: (0, 2.5, 0)

The wind tunnel opening is at a location of approximately -1.5 m on the x axis. The height (along z axis) and width (along y axis) of the tunnel opening are approximately 3 m. The trajectory with respect to the windtunnel opening are drawn in figure 2. The wind speed direction is along the negative direction of the y axis flowing from the wind tunnel opening towards the drone.

2.3. Measuring performance

The tuning of both control algorithms was with similar response in attitude and position control in no-wind conditions.

To really observe the performance difference between the two algorithms, it is important to look at both the absolute error, as well as the time it takes to recover from the wind gust disturbance. For that, we look at the 'absolute maximum position error' in meter e_{max} when entering the wind gust. To measure relative performance of INDI and PID, we take the ratio of the two to get our first metric *relative maximum position error*:

$$e_{rel} = \frac{e_{maxPID}}{e_{maxINDI}} \tag{1}$$

A measure that also takes into account the recovery time of the position is the integral of the error over time, where the position of the drone is in front of the wind:

$$I = \Sigma(e * \Delta t) \tag{2}$$

With *int* having unit $[m * s]$ and Δt is the time step between the samples.
Calculating the ratio between the two integrated errors for both INDI and PID results in our second metric, the relative integrated error:

$$I_{rel} = \frac{int_{PID}}{int_{INDI}} \tag{3}$$

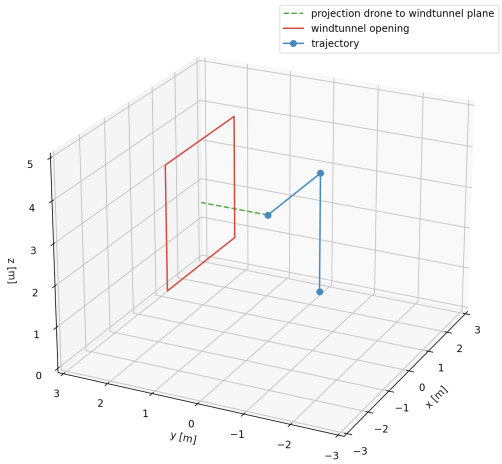

Figure 2: Drone trajectory with respect to the wind tunnel opening

3. Results

Figure 3 shows position error due to wind in Y direction, as well as the movement in and out of the airflow in X direction for both INDI and PID, for a wind speed of 20 m/s. For a 20 m/s wind gust the maximum absolute error when entering the wind gust for INDI is $0.37m$, for PID is $0.62m$. Using the metrics from equations 1 and 3 we find that

$$e_{rel} = 1.67,\ I_{rel} = 9.45$$

This means that the maximum error using PID is 1.67 times larger compared to INDI, and that the cumulative error while in the wind using PID is 9.45 times larger compared to INDI.

The results of all wind speeds is available in table 1.

For visualization of the flight path of both algorithms, figure 4 shows a top view of the wind tunnel and the flight paths at 20m/s wind speeds. The figures for wind gust rejection and top views can be found in Appendix A.

At the highest wind speed of 25 m/s, INDI is able to recover after a maximum position error of approximately 1 meter. PID is not able to recover its position, and battles the wind gust until the battery is depleted.

Table 1: Results

Windspeed	max error PID	max error INDI	rel error	integrated error PID	integrated error INDI	relative integrated error
10 m/s	0.17	0.13	1.37	0.82	0.17	4.69
15 m/s	0.3	0.23	1.34	2.86	0.31	9.23
20 m/s	0.62	0.37	1.68	5.06	0.54	9.45
25 m/s	5.17	1.07	4.82	74.44	3.39	21.99

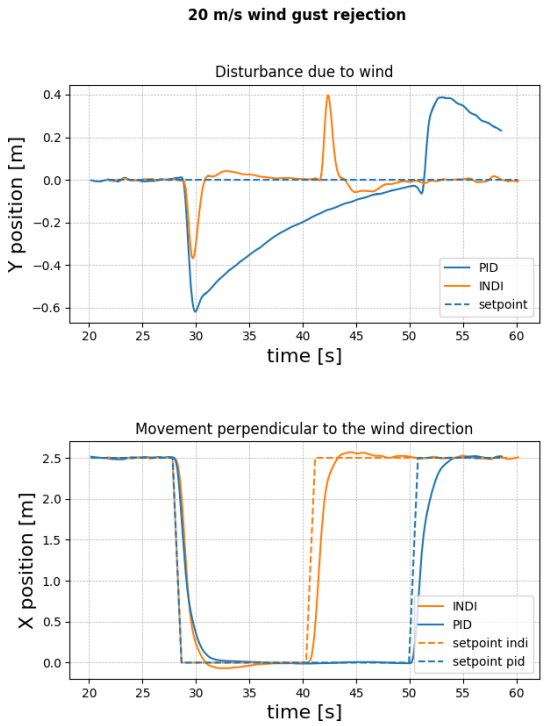

Figure 3: Drone trajectory with respect to the wind tunnel opening

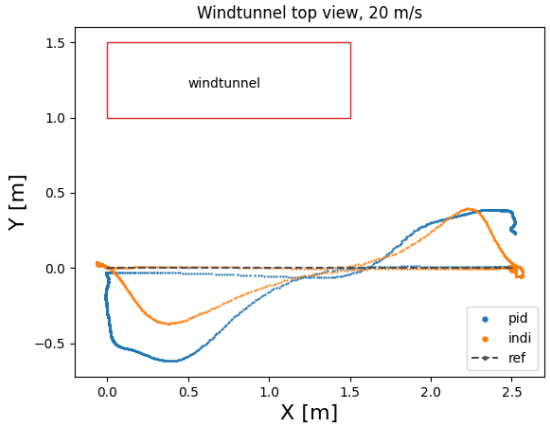

Figure 4: Top view of the windtunnel

4. Discussion

Figure 3 shows disturbance in Y direction due to wind for INDI as well as PID for a 20 m/s wind speed. The disturbance is visible as soon as the X position of the drone is in front of the wind tunnel opening.
The waypoint in the center of the wind turbine has a hold time of 10s with an acceptance radius of 20cm. The acceptance radius is the distance from the target setpoint for which the flight controller deems the setpoint reached. The hold time will start counting when the drone is within that acceptance radius. The drone using the PID controller reaches the acceptance radius distance at approximately 40 seconds, causing the new setpoint to be activated at approximately 50 seconds. INDI reaches this acceptance radius 10 seconds earlier, at around approximately 30 seconds.
It is interesting to see that the relative maximum position error metric e_{rel} is similar for 10 m/s (figure A.5) and 15 m/s wind speeds (figure A.7). However, PID takes longer to correct for the disturbance at 15 m/s than at 10 m/s, which is nicely reflected by the second metric, the integrated error. For 10 m/s this is 4.69, while for 15 m/s this is 9.23, almost double.
At 25 m/s, INDI is able to recover while PID is not. This shows that INDI enables drones to fly in more extreme weather conditions.

One of the explanations for the slower recovery time of PID is that PID uses an integrator term to correct for the wind gust. Integrator terms are similar to buffers that have to fill up over time. Increasing the integrator term to correct faster is an option, however a trade off is always present. An integrator term that is too high can induce other unwanted flight behaviour. INDI is inherently different and is known to have faster disturbance rejection. This is clearly reflected in the test results: INDI outperforms PID at every wind speed, and the higher the wind speed, the larger the difference in performance between INDI and PID is.

5. Conclusion and Recommendations

5.1. Conclusion

This experiment shows the different behaviours in wind gust rejection for a common PID flight control algorithm and Fusion Reflex's INDI algorithm. Both flight control algorithms run on the same Fusion Reflex hardware, on the same multirotor platfrom.

The metrics used to analyse wind gust rejection are 'relative maximum position error' e_{rel}, and 'relative integrated error' I_{rel}. The first metric e_{rel} looks at the maximum position deviation due to the intial wind gust. The second metric I_{rel} integrates the error over time and thus takes into account the recovery time of the drone to its position setpoint. The experiment was run at 10 m/s, 15 m/s, 20 m/s and 25 m/s. INDI outperforms PID at every windspeed, both in e_{rel} as in I_{rel}. The higher the windspeed, the larger both metrics become, indicating that benefit of INDI increases with windspeed.

5.2. Recommendations

The tuning of a flight control algorithm will determine the flight response. PID has an integrator term that is chosen with a tradeoff. The integrator term is important for external perturbations, but setting this term too high can cause unwanted flight behaviour. In a next experiment, it would be interesting too see just how the increase/decrease of the integrator term affects flight behaviour of the drone.

The maximum bank angle limit was set to 45 degrees in this experiment for both flight control algorithms. Increasing this maximum bank angle limit would potentially result in faster response times for both algorithms.

Appendix A. Appendix A

Appendix A.1. 10 m/s wind speeds

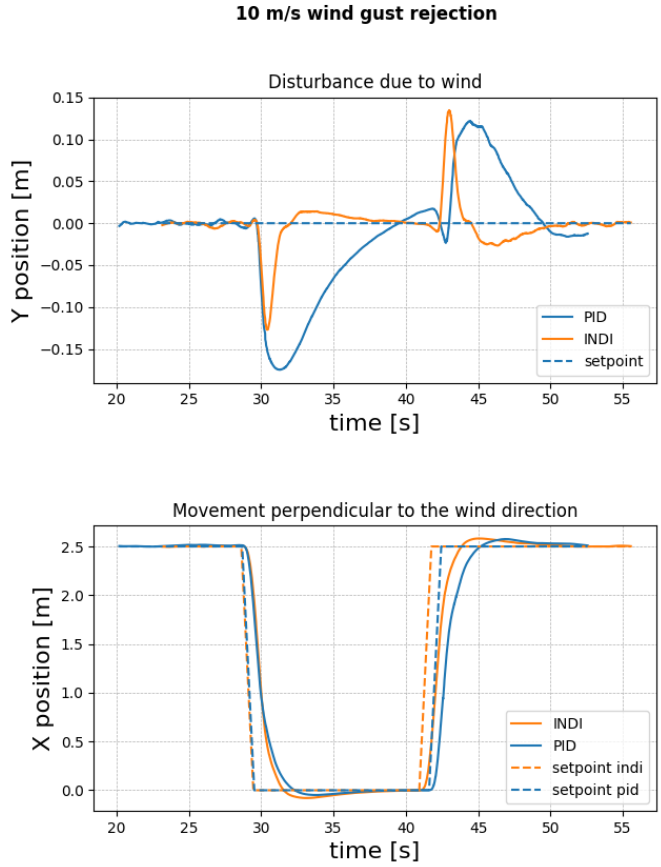

Figure A.5: Drone position in X and Y direction over time

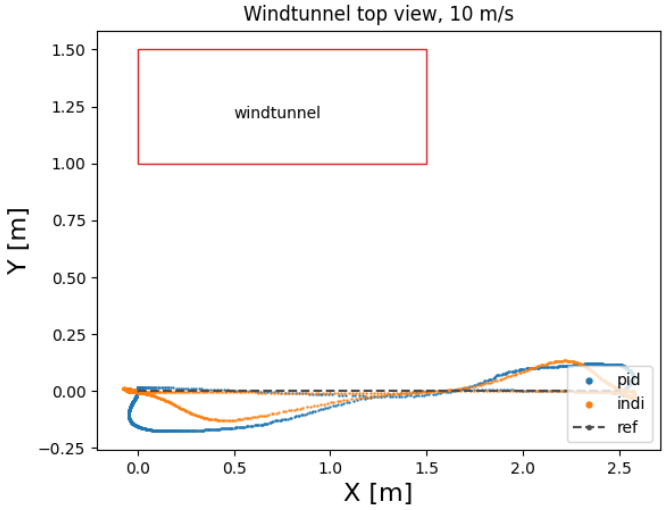

Figure A.6: Top view of the wind tunnel

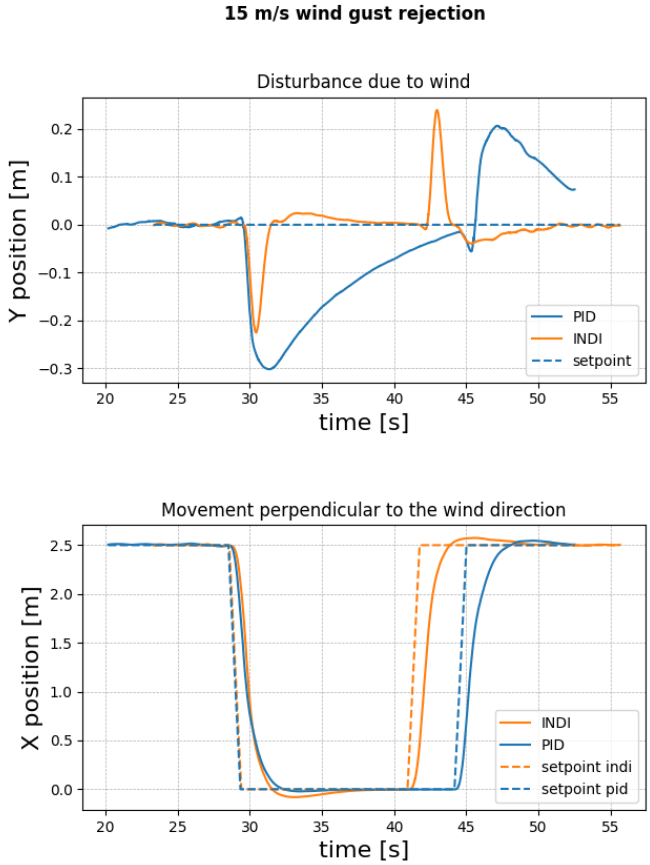

Figure A.7: Drone position in X and Y direction over time

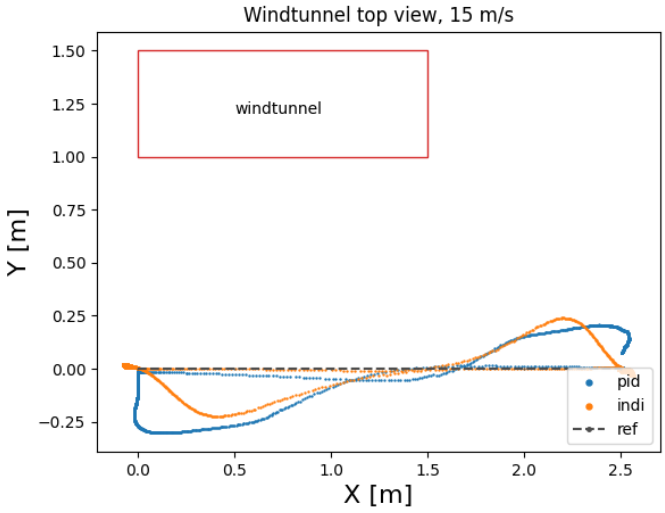

Figure A.8: Top view of the wind tunnel

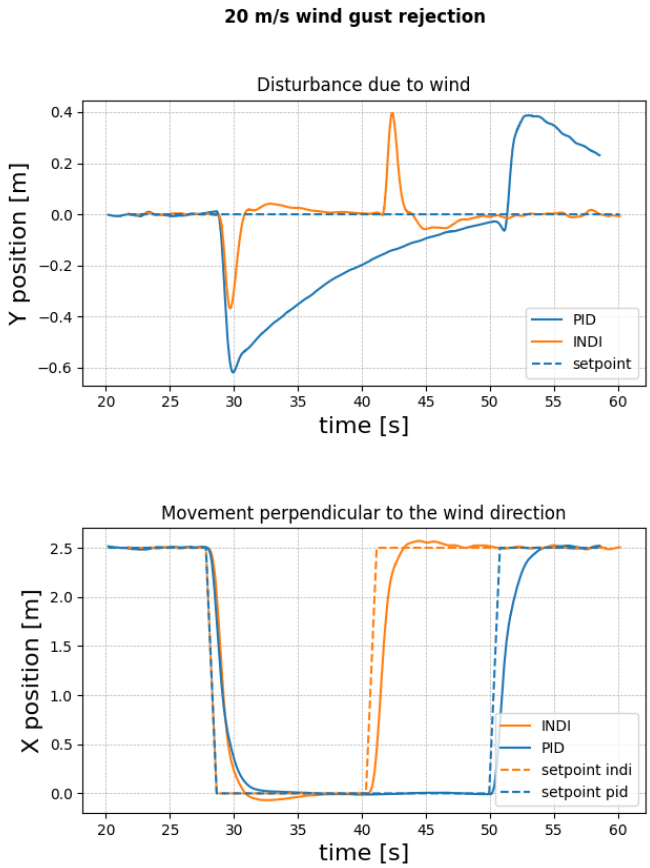

Figure A.9: Drone position in X and Y direction over time

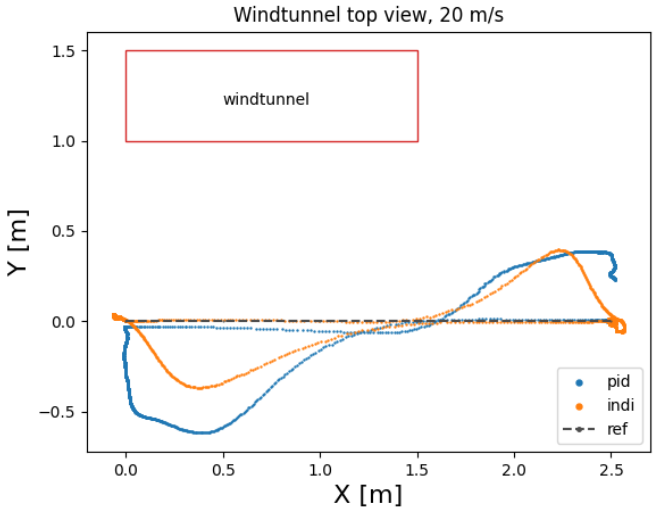

Figure A.10: Top view of the wind tunnel

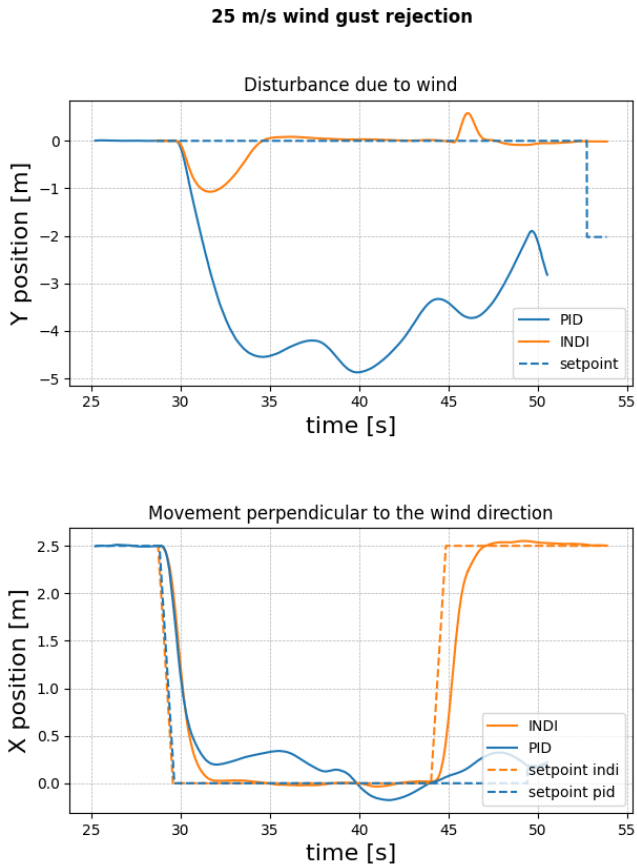

Figure A.11: Drone position in X and Y direction over time

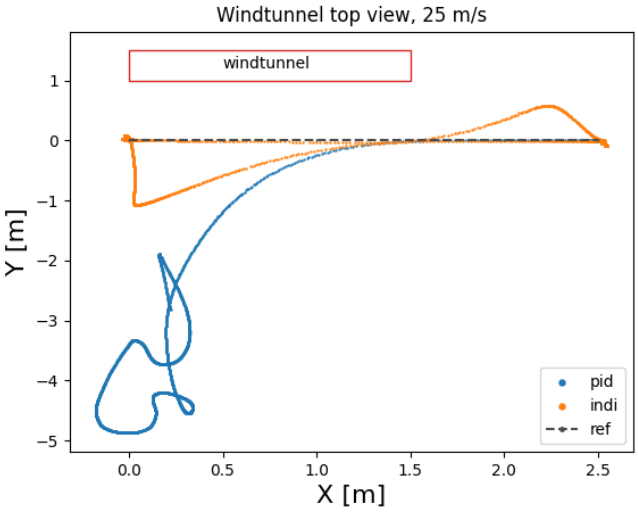

Figure A.12: Top view of the wind tunnel